ACS Photonics

pubs.acs.org/journal/apchd5

Letter

Optically Controlled Spin Gate Using GaN Quantum Dots

Juhyeon Kim, Zachary Croft, Duncan G. Steel, and Pei-Cheng Ku*

Cite This: *ACS Photonics* 2022, 9, 1529−1534

Read Online

ACCESS | Metrics & More | Article Recommendations | Supporting Information

ABSTRACT: Two laterally positioned quantum dot single-photon emitters in different semiconductor heterostructures were analyzed. A controlled phase gate between two quantum dot spins was shown based on the Coulomb interaction between the two quantum dot trions. The interaction shifts the bitrion energy manifold, enabling a π-phase shift to be acquired depending on the state of the control qubit. The gate fidelity increases with an increasing bitrion coupling which in turn depends on the spacing between the quantum dots. In practical applications, this spacing needs to be sufficiently large to allow the two-quantum-dot system to be fabricated. An enhanced bitrion coupling was shown in In(Ga)N quantum dots both in a bulk GaN matrix and in a dot-in-wire geometry, compared to that in In(Ga)As dots. The enhanced bitrion coupling in In(Ga)N dots increases the edge-to-edge interdot spacing needed to achieve the same gate performance, allowing a deterministic spin−spin gate to be designed based on site-controlled dot-in-wire In(Ga)N quantum dots that can be readily fabricated with an interdot spacing of 10 nm using state-of-the-art lithography.

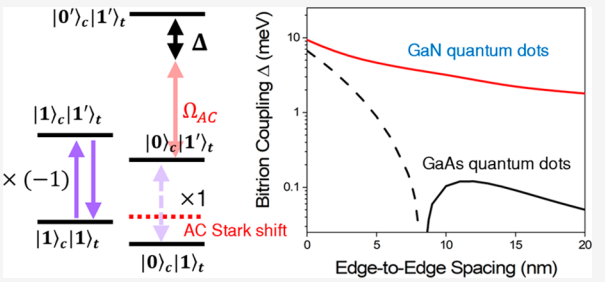

KEYWORDS: *Single Photon Emitters, Coulomb Interaction, Trions, Bitrions, Semiconductor quantum dots, Quantum Gates*

The qubit is the fundamental building block for quantum information. The ability to generate, process, and store qubits establish the foundation for quantum information science and technologies. Isolated electron spins have robust coherence and are a promising qubit candidate for a solid-state quantum system.[1,2] In semiconductors, electron spins can be isolated using a gate-defined[3] or heterostructural quantum dot.[4] In this work, we focus on single electron spins confined in semiconductor quantum dot heterostructures as the qubits. We will refer to these structures simply as quantum dots in the following discussions. Quantum dot spin qubits can be easily interfaced with photonic (flying) qubits using a negatively charged quantum dot excited to a trion state, making it especially attractive for quantum network applications.[5] The radiative decay of the trion state creates a single photon whose polarization is entangled to the spin as a result of the optical selection rule.[6,7] Significant advances have been made in optically manipulating spins in In(Ga)As/GaAs quantum dots, including the initialization and single-qubit operations.[6,8] Further extension of the ability for a two-qubit gate is crucial to enable more versatile quantum computational functionalities,[9] for example, entanglement swapping in a quantum link[10−12] and generation of large-scale entangled cluster state.[13]

Various proposals have been made to couple two spin qubits in two separate quantum dots. Examples of the couplings include electromagnetic coupling,[14,15] exchange interaction,[16−18] and Coulomb interaction.[19] Specifically, a two-qubit gate using the exchange interaction between two vertically coupled quantum dots has been experimentally demonstrated.[4] However, vertically coupled quantum dots present technological challenges of precisely controlling the energy levels and individually performing single-qubit operations. It is also difficult to be scaled to a large qubit network.[20] In contrast, laterally coupled quantum dots can be separately biased with two electrical contacts. Yet, coupling between two lateral quantum dots has only been shown in gate-defined quantum dots and has not been systematically studied in heterostructural quantum dots.[21] The electron wave functions are tightly confined in heterostructural quantum dots, requiring a much smaller interdot spacing to achieve a sufficient coupling strength. No known fabrication processes have been reported to date that can controllably place two In(Ga)As quantum dots within such proximity.[22] In this work, we propose to use In(Ga)N quantum dots to overcome this limitation. We will demonstrate that the interdot spacing required to achieve a significant coupling to enable a two-qubit controlled phase (CZ) gate can be increased by an order of magnitude, allowing two site-controlled In(Ga)N quantum dots to be deterministically placed. We will show that the underlying mechanisms contributing to a greatly enhanced Coulomb coupling between two In(Ga)N quantum dots compared to between two In(Ga)As dots include a low dielectric constant matrix, a strong

Received: January 14, 2022
Published: April 15, 2022

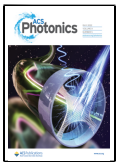

https://doi.org/10.1021/acsphotonics.2c00083
ACS Photonics 2022, 9, 1529−1534

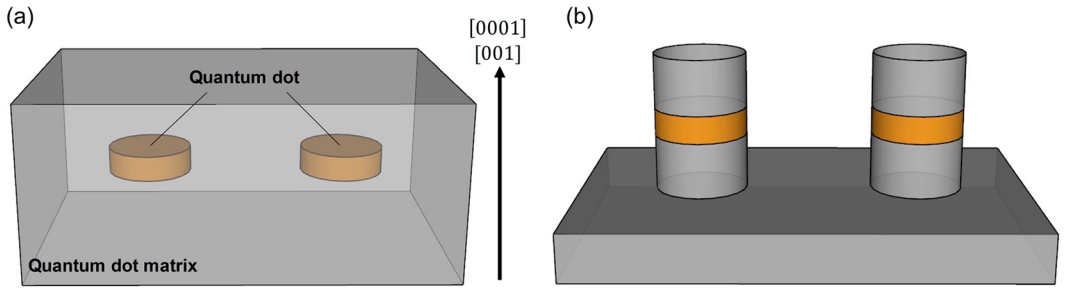

Figure 1. Schematic of two quantum dot heterostructures considered in this work. (a) Two quantum dots are laterally positioned in a bulk matrix. The dots are assumed to be disk-shaped with a diameter of 10 nm and on the (0001) plane for In(Ga)N dots and (001) plane for In(Ga)As dots. (b) Two quantum dots, each embedded in a nanowire structure, laterally positioned and surrounded by air. The nanowire is along the [0001] or [001] axis for In(Ga)N and In(Ga)As dots, respectively. In the case of In(Ga)N dots, the strain relaxation around the nanowire's circumference creates a radial confinement potential to confine the electrons at the center of the dot. Two different nanopillar diameters are considered: 10 and 20 nm.

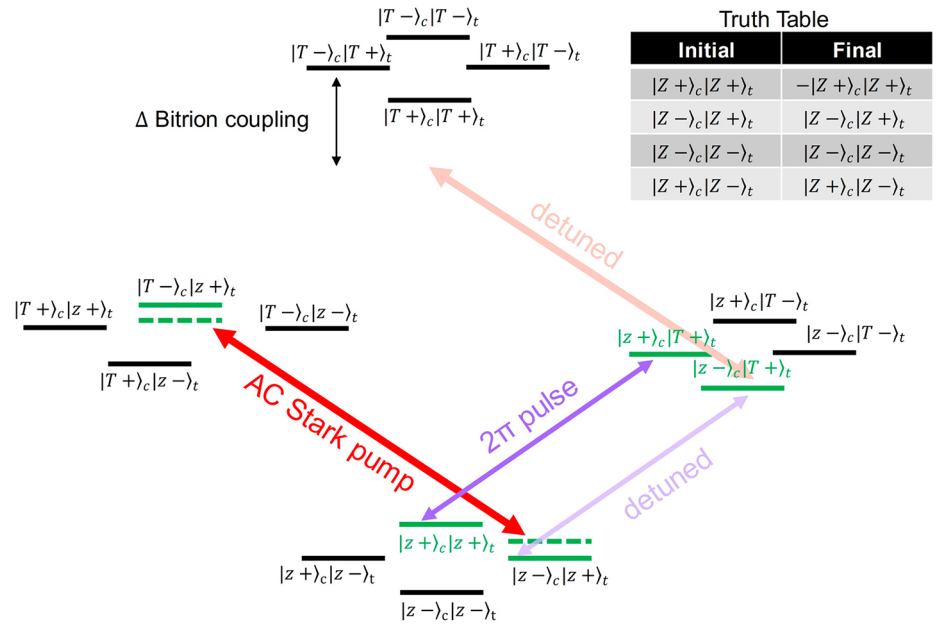

Figure 2. Illustration of the CZ gate utilizing the Coulomb coupling between two laterally positioned quantum dots. The coupling forms a 16-level Hamiltonian. We assume a Faraday configuration with a nonzero magnetic field along the [0001]/[001] or z direction. The spin eigenstates are denoted as $|z+\rangle$ and $|z-\rangle$, which are nondegenerate. The subscripts c and t denote the control and target dots, respectively. The schematic shown here is for a CZ gate with a truth table shown on the right. The gate operates with two lasers, including a 2π pulse (purple arrows) applied in resonance with the target dot's $|z+\rangle$ to $|T+\rangle$ transition and a strong pump (red arrows) detuned from the control dot's $|z-\rangle$ to $|T-\rangle$ transition by several line widths. The strong pump induces the AC Stark effect, which shifts the energy levels of $|z-\rangle_c|z+\rangle_t$ and $|T-\rangle_c|z+\rangle_t$. The bitrion coupling Δ suppresses the AC Stark effect on levels $|z-\rangle_c|T+\rangle_t$. Hence, the lower purple arrow is not in resonance and will not generate a phase shift for $|z-\rangle_c|z+\rangle_t$. The other two states $|z+\rangle_c|z-\rangle_t$ and $|z-\rangle_c|z-\rangle_t$ will not be affected because of either detuning or polarization selection rules.

piezoelectric effect, and the large electron and hole effective masses.

GaN semiconductors have a wurtzite symmetry and, as a result, exhibit a strong piezoelectric field along the [0001] direction. We consider two laterally adjacent In(Ga)N quantum dots grown on the (0001) crystal plane. The piezoelectric field slightly misaligns the electron and hole wave functions, creating a permanent dipole moment. In our studies, we assumed the quantum dot was disk-shaped with a height of 3 nm. The dot's diameter was set as a variable. We also considered two types of heterostructures to represent two different fabrication methods. Figure 1a shows two In(Ga)N quantum dots in a bulk GaN matrix, typically formed by a Stranski–Krastanow growth[23] or a capillary effect.[24,25] Figure 1b shows two In(Ga)N dot-in-wire (DIW) structures, which can be formed either by catalyst-assisted bottom-up growth[26,27] or by lithography and etching.[28−30] The top-down lithography process has a better scalability beyond two dots, while the Stranski–Krastanow process to date still produces the highest quality dots with a narrow line width. The two dots were assumed to be individually gated. Both dots are assumed to be charged with one electron in the conduction band, for example, using a pn junction structure, as previously demonstrated in ref 31. We assumed the indium composition to be 20%.

We first describe the protocol of the CZ gate utilizing the Coulomb coupling between the two quantum dots, inspired by the work of Saikin et al. in ref 19 in which the preparation of a highly entangled state between two quantum dot spins was shown. Figure 2 shows the energy manifold formed by the coupled dot system. Without loss of generality, we assume one dot has a higher energy than the other dot. This assumption

https://doi.org/10.1021/acsphotonics.2c00083
ACS Photonics 2022, 9, 1529−1534

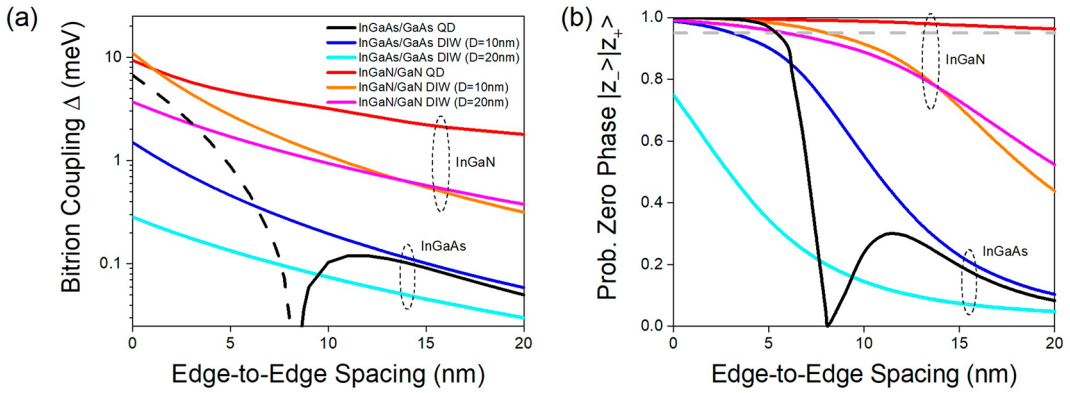

Figure 3. (a) Bitrion coupling Δ for various quantum dot structures in two different types of heterostructures shown in Figure 1. Δ was obtained from a first-order perturbation theory using wave functions calculated from the k-dot-p method. Exchange interaction was included with proper antisymmetrization of the wave functions. The interdot spacing shown here is the shortest edge-to-edge distance between the two dots. The dot diameter is 10 nm unless otherwise specified in the parentheses. The indium composition is 20% in all structures. The dashed portion of the curve represents a negative Δ plotted with its absolute value. (b) The CZ gate's performance for various quantum dot structures defined in (a). The curves use the same color coding scheme as in (a). A shown here is the probability to suppress the undesired π phase shift for the state $|z-\rangle_c|z+\rangle_t$. The dashed line corresponds to a 95% probability. See Supporting Information for the density matrix model and parameters used for the numerical calculations. For DIW dots, we used the line width of the bulk dots in the calculations, although we wish to point out that the fabrication technology is still in its infancy and the current line width is considerably larger than the bulk dots' value.

also resembles the practical situation in which it is nearly impossible to fabricate two identical dots. The different resonances also enable one to optically address each of the two dots separately. The Coulomb interaction between the two dots forms a 16-level Hamiltonian. We have assumed the effect of Coulomb coupling was relatively small. While there may be some mixing of the states due to the interaction, the same angular momentum states are maintained for the simplicity of the discussion. We denote the quantum dot ground and excited (trion) states by $|z\pm\rangle$ and $|T\pm\rangle$, respectively, where + and − are the spin eigenstates in the [0001] direction, and excitation is achieved using circularly polarized light $\sigma_\pm$ with the following selection rules: $|z\pm\rangle \xrightarrow{\sigma_\pm} |T\pm\rangle$. In Figure 2, the manifold is drawn by assuming a nonzero magnetic field in the Faraday geometry ($B_z \neq 0$) such that $|z+\rangle$ and $|z-\rangle$ are nondegenerate. We further label the state by subscripts c and t to denote the control and target dots, respectively. For example, $|z+\rangle_c|z-\rangle_t$ denotes the control dot is in the $|z+\rangle$ state and the target dot is in the $|z-\rangle$ state.

The proposed CZ gate changes the phase of $|z+\rangle_c|z+\rangle_t$ by π. When a 2π pulse is applied in resonance with the target dot's $|z+\rangle_t \rightarrow |T+\rangle_t$ transition, both $|z-\rangle_c|z+\rangle_t$ and $|z+\rangle_c|z+\rangle_t$ can acquire a π-phase shift. All other transitions will be either out of resonance or forbidden by the polarization selection rule and will not be affected. To suppress the phase shift of the state $|z-\rangle_c|z+\rangle_t$, we simultaneously apply a strong pulse slightly detuned from the control dot's $|z-\rangle_c \rightarrow |T-\rangle_c$ transition by a few line widths. The AC Stark effect shifts the energy of $|z-\rangle_c|z+\rangle_t$. In the absence of any interdot coupling, the state $|z-\rangle_c|T+\rangle_t$ will be shifted by the same amount, keeping $|z-\rangle_c|z+\rangle_t \rightarrow |z-\rangle_c|T+\rangle_t$ still in resonance with the 2π pulse. However, when there exists a strong Coulomb coupling between the two dots, the bitrion sector of the energy manifold in Figure 2 is shifted by Δ, suppressing the AC Stark effect's influence on the $|z-\rangle_c|T+\rangle_t \rightarrow |T-\rangle_c|T+\rangle_t$ transition. As a result, the transition $|z-\rangle_c|z+\rangle_t \rightarrow |z-\rangle_c|T+\rangle_t$ will be detuned from the 2π pulse, and the state $|z-\rangle_c|z+\rangle_t$ will not acquire a phase shift.

The energy shift Δ induced by the bitrion coupling needs to be sufficiently large to avoid the AC Stark effect to suppress the unwanted π-phase shift for the state $|z-\rangle_c|z+\rangle_t$. In the case of two lateral quantum dots, the coupling includes both the Coulomb and exchange interactions. The energy shift Δ can be determined using the first-order perturbation theory as follows:

$$\Delta = 3|E^{ee}| - 4|E^{eh}| + |E^{hh}| \tag{1}$$

where

$$E_{jk} = \langle \psi_{ct}^{jk} | \hat{V} | \psi_{ct}^{jk} \rangle \qquad j, k \in \{e, h\} \tag{2}$$

and

$$\hat{V} = q_c q_t / 4\varepsilon\varepsilon_0 r \tag{3}$$

In the above equations, $q_{c,t}$ is the electric charge of either the electron and hole, ε is the dielectric constant of the quantum dot matrix, $\varepsilon_0 = 8.85 \times 10^{-12}$ F/m, e and h denote the electron and hole, respectively, and $r = |\hat{r}_c - \hat{r}_t|$, where $\hat{r}_c$ and $\hat{r}_t$ are the position operators for the control and target dots, respectively. In eq 1, the first coefficient 3 comes from the four pairwise interactions between the four electrons (two in each dot) subtracting the ground-state interaction (1 electron in each dot). The exchange interaction is included by antisymmetrizing the wave functions ψ_{ct}^{ee} and ψ_{ct}^{hh} as follows:

$$\psi_{ct}^{kk}(r_c, r_t) = \frac{1}{\sqrt{2}}(\psi_c^k(r_c)\psi_t^k(r_t) - \psi_c^k(r_t)\psi_t^k(r_c)) \qquad k \in \{e, h\} \tag{4}$$

We calculated the wave functions using the 8-band k-dot-p method, but ignored the conduction-valence band coupling, a good approximation for GaN semiconductors.[32] We also ignored the random alloy and excitonic effects.[33] These effects can slightly modify the wave functions and shift the energy levels. The energy shift is intrinsic to each dot and does not affect the bitrion coupling Δ. The modification of wave functions will have an impact on Δ. However, as the change of the wave function occurs in a length scale considerably less than the interdot spacing of interest here, we expect the impact will not significantly alter the conclusion of this study. The similar argument applies to the quantum dot shape. The actual

https://doi.org/10.1021/acsphotonics.2c00083
ACS Photonics 2022, 9, 1529−1534

shape of the quantum dot depends on the growth condition and fabrication method. For example, Stranski−Krastanow dots resemble a truncated pyramidal shape, somewhere between a disk and a pyramid. Figure S1 compares Δ between disk- and pyramidal-shaped dots. The difference in Δ is within a factor of 2 and the trends of Δ versus the interdot spacing are identical.

Figure 3a shows the bitrion coupling Δ for the two In(Ga)N quantum dot heterostructures. For comparison, we calculated Δ between two disk-shaped In(Ga)As quantum dots in a GaAs matrix. Δ is positively defined when the bitrion sector moves toward a higher energy. A dashed curve represents a negative Δ. Although not technologically viable, we also included the comparison to an In(Ga)As DIW structure to elucidate the physics behind the enhancement of Coulomb coupling in In(Ga)N quantum dots. To deterministically place two quantum dots, it is crucial that the interdot spacing is greater than the lithographic resolution, preferably in the range of 10−20 nm or larger. Figure 3a suggests that the bitrion coupling in In(Ga)N quantum dots is an order of magnitude larger than that in In(Ga)As quantum dots regardless of the type of heterostructures. To suppress the AC Stark effect on the $|z-\rangle_c|z+\rangle_t \rightarrow |z-\rangle_c|T+\rangle_t$ transition, we need Δ to be at least a few line widths away from the AC Stark laser. Based on the best reported homogeneously broadened line widths for self-assembled quantum dots in a bulk matrix,[34,35] the minimum Δ's are ∼0.7 and ∼1.5 meV for In(Ga)As and In(Ga)N quantum dots, respectively to suppress the π-phase shift for the state $|z-\rangle_c|z+\rangle_t$ with a probability of 95% (Figure 3b; defined by the projection of $|z-\rangle_c|z+\rangle_t$ to itself without any phase shift; see Supporting Information for the simulation details). These values correspond to a minimum edge-to-edge interdot spacing of 5 nm for In(Ga)As dots in a bulk GaAs matrix and several tens of nanometers for In(Ga)N dots in a bulk GaN matrix. The line widths for DIW dots today are still much wider due to inhomogeneous broadening such as spectral diffusion. The true homogeneous line width of a DIW dot is not yet clear, but further material improvements are likely necessary to use the DIW dots for practical applications.

To understand the origin of the enhanced Coulomb coupling between two In(Ga)N quantum dots, we investigated the effects of their three major differences from In(Ga)As dots: a strong piezoelectric field along the [0001] direction, a large effective mass for both electrons and holes, and a lower dielectric constant of the quantum dot matrix. We investigated the evolution from two In(Ga)As dots in a bulk GaAs matrix to two In(Ga)N dots in a bulk GaN matrix. The results are shown in Figure 4a. First, we looked at the effect of the effective masses by using the In(Ga)N electron and hole wave functions in the calculation of Δ for the In(Ga)As dots. We artificially "turned off" the piezoelectric effect by vertically aligning the electron and hole wave functions. Because of the larger effective masses for both electrons and holes in GaN, the wave functions, especially the holes', are much more spatially confined. This leads to a weaker exchange interaction when compared to the In(Ga)As dots. But it also increases the distance between the electron in one dot and the hole in the other dot because of the tightly confined hole wave function. The result is a smaller Coulomb interaction term $|E^{eh}|$ in eq 1 and an increase of Δ. Besides the In(Ga)N quantum dots considered here, GaN/AlN as well as most II−VI colloidal quantum dots such as CdSe/ZnS and CdSe/CdS[36,37] exhibit

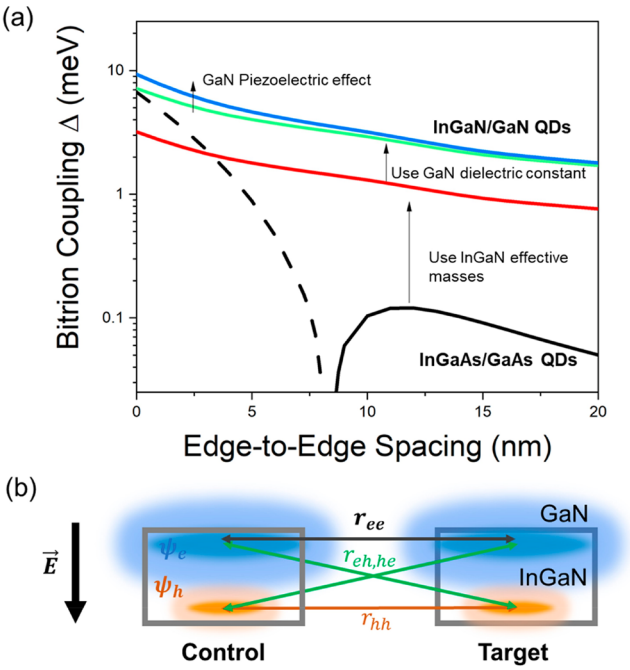

Figure 4. (a) Evolution from In(Ga)As/GaAs quantum dots to In(Ga)N/GaN quantum dots to illustrate the mechanisms underlying the enhanced Coulomb coupling between the In(Ga)N dots. From bottom to top, the first line shows Δ for In(Ga)As/GaAs quantum dots. The second line uses wave functions obtained from In(Ga)N/GaN quantum dots, but artificially turns off the piezoelectric effect. The third line replaces the GaAs matrix with GaN but without recalculating the wave functions. The top line shows Δ for In(Ga)N/GaN quantum dots. (b) Illustration of the piezoelectric effect's role on Δ. The misalignment of the electron and hole wave functions due to the piezoelectric field $\vec{E}$ along the $[000\bar{1}]$ direction increases the distance between the electron in one dot and the hole in the other dot r_{eh} and r_{he}. The larger distance reduces the Coulomb coupling $|E^{eh}|$ and enhances the bitrion coupling given in eq 1. The piezoelectric effect has a stronger effect on Δ when the interdot spacing is small. At a large interdot spacing, r_{eh} or r_{he} are approximately equal to r_{ee} or r_{hh}. Therefore, the piezoelectric effect's influence on Δ becomes negligible.

similar properties and are expected to also be a good candidate for the proposed spin−spin gate.

Next, we changed the dielectric constant of the GaAs matrix to GaN, which is roughly half of that of GaAs, while keeping the piezoelectric effect off. This doubles the Δ, which agrees with eq 3. Finally, we restored the piezoelectric effect and observed a slight increase of Δ in Figure 4a. We explain the increase using the schematic in Figure 4b. The piezoelectric field separates the electron and hole wave functions in the [0001] direction. It has a similar effect to Δ as the effective mass, increasing the distance between the electron in one dot and the hole in the other. Comparing the three effects in Figure 4a, we can see that the effective mass has the largest impact on the increase of Δ, followed by the dielectric constant of the matrix. The piezoelectric effect has a larger impact for a small interdot spacing when the slightly larger distance between the electron and hole in neighboring dots has more significance compared to the interdot spacing. But as the interdot spacing becomes larger, the effect becomes negligible.

In summary, we have proposed and shown a viable spin−spin CZ gate between two quantum dot single-photon emitters. The gate operation is enabled by the Coulomb

https://doi.org/10.1021/acsphotonics.2c00083
ACS Photonics 2022, 9, 1529−1534

interaction that only couples the two dots when both dots are in their excited trion states. The transient coupling does not couple the ground-state wave functions, allowing the two quantum dot spins to be independently initialized, tuned, and processed. In the Faraday's geometry, when a control pulse is in resonant with the target dot's $|z+\rangle$ state, the bitrion coupling can selectively suppress the π phase shift depending on the control dot's spin state with the assistance of a strong pump laser to induce the AC Stark effect. With the bitrion energy levels shifted away by the interdot coupling, the AC Stark laser can suppress the phase shift that would have been acquired by the target dot's $|z+\rangle$ state when the control dot is in the $|z-\rangle$ state. It was shown that the coupling can be enhanced by an order of magnitude between the In(Ga)N quantum dots compared to In(Ga)As dots as a result of highly confined electron and hole wave functions, a lower dielectric constant of the quantum dot matrix, and to a lesser extent the existence of a strong piezoelectric field. While In(Ga)N quantum dots' line width is 10× that of In(Ga)As dots, the much tighter confinement of GaN dots' wave functions leads to a 30× interdot coupling to enable a larger dot-to-dot spacing. A spacing as large as tens of nanometers between two In(Ga)N quantum dots in a bulk GaN matrix can achieve a successful gate operation at a probability of 95% as compared to 5 nm for In(Ga)As dots. For In(Ga)N DIW structures, the line width currently is still much larger than that of bulk In(Ga)N dots. With the continuing improvement of the material quality, In(Ga)N quantum dots can become a viable platform for quantum information applications.

■ ASSOCIATED CONTENT

Supporting Information

The Supporting Information is available free of charge at https://pubs.acs.org/doi/10.1021/acsphotonics.2c00083.

Comparison of disk- and pyramidal-shaped quantum dot results and density of matrix simulations of the gate operation (PDF)

■ AUTHOR INFORMATION

Corresponding Author

Pei-Cheng Ku − *Department of Electrical Engineering and Computer Science, University of Michigan, Ann Arbor, Michigan 48109, United States; Applied Physics Program, University of Michigan, Ann Arbor, Michigan 48109, United States;* orcid.org/0000-0003-2282-5954; Email: peicheng@umich.edu

Authors

Juhyeon Kim − *Department of Electrical Engineering and Computer Science, University of Michigan, Ann Arbor, Michigan 48109, United States*

Zachary Croft − *Applied Physics Program, University of Michigan, Ann Arbor, Michigan 48109, United States*

Duncan G. Steel − *Department of Electrical Engineering and Computer Science, University of Michigan, Ann Arbor, Michigan 48109, United States; Applied Physics Program, University of Michigan, Ann Arbor, Michigan 48109, United States*

Complete contact information is available at: https://pubs.acs.org/10.1021/acsphotonics.2c00083

Funding

National Science Foundation ECCS 1838996.

Notes

The authors declare no competing financial interest.

■ ACKNOWLEDGMENTS

The data that support the findings of this study are available from the corresponding author upon reasonable request.

■ REFERENCES

(1) Loss, D.; DiVincenzo, D. P. Quantum Computation with Quantum Dots. *Phys. Rev. A* **1998**, *57* (1), 120−126.

(2) Xu, X.; Yao, W.; Sun, B.; Steel, D. G.; Bracker, A. S.; Gammon, D.; Sham, L. J. Optically Controlled Locking of the Nuclear Field via Coherent Dark-State Spectroscopy. *Nature* **2009**, *459* (7250), 1105−1109.

(3) Petta, J. R.; Johnson, A. C.; Taylor, J. M.; Laird, E. A.; Yacoby, A.; Lukin, M. D.; Marcus, C. M.; Hanson, M. P.; Gossard, A. C. Coherent Manipulation of Coupled Electron Spins in Semiconductor Quantum Dots. *Science* **2005**, *309* (5744), 2180−2184.

(4) Kim, D.; Carter, S. G.; Greilich, A.; Bracker, A. S.; Gammon, D. Ultrafast Optical Control of Entanglement between Two Quantum-Dot Spins. *Nat. Phys.* **2011**, *7* (3), 223−229.

(5) Warburton, R. J. Single Spins in Self-Assembled Quantum Dots. *Nat. Mater.* **2013**, *12* (6), 483−493.

(6) Gao, W. B.; Fallahi, P.; Togan, E.; Miguel-Sanchez, J.; Imamoglu, A. Observation of Entanglement between a Quantum Dot Spin and a Single Photon. *Nature* **2012**, *491* (7424), 426−430.

(7) Schaibley, J. R.; Burgers, A. P.; McCracken, G. A.; Duan, L.-M.; Berman, P. R.; Steel, D. G.; Bracker, A. S.; Gammon, D.; Sham, L. J. Demonstration of Quantum Entanglement between a Single Electron Spin Confined to an InAs Quantum Dot and a Photon. *Phys. Rev. Lett.* **2013**, *110* (16), 167401.

(8) Kim, H.; Bose, R.; Shen, T. C.; Solomon, G. S.; Waks, E. A Quantum Logic Gate between a Solid-State Quantum Bit and a Photon. *Nat. Photonics* **2013**, *7* (5), 373−377.

(9) Sleator, T.; Weinfurter, H. Realizable Universal Quantum Logic Gates. *Phys. Rev. Lett.* **1995**, *74* (20), 4087−4090.

(10) Bennett, C. H.; Brassard, G.; Crépeau, C.; Jozsa, R.; Peres, A.; Wootters, W. K. Teleporting an Unknown Quantum State via Dual Classical and Einstein-Podolsky-Rosen Channels. *Phys. Rev. Lett.* **1993**, *70* (13), 1895−1899.

(11) Duan, L.-M.; Lukin, M. D.; Cirac, J. I.; Zoller, P. Long-Distance Quantum Communication with Atomic Ensembles and Linear Optics. *Nature* **2001**, *414* (6862), 413−418.

(12) Basso Basset, F.; Rota, M. B.; Schimpf, C.; Tedeschi, D.; Zeuner, K. D.; Covre Da Silva, S. F.; Reindl, M.; Zwiller, V.; Jöns, K. D.; Rastelli, A.; Trotta, R. Entanglement Swapping with Photons Generated on Demand by a Quantum Dot. *Phys. Rev. Lett.* **2019**, *123* (16), 160501.

(13) Economou, S. E.; Lindner, N.; Rudolph, T. Optically Generated 2-Dimensional Photonic Cluster State from Coupled Quantum Dots. *Phys. Rev. Lett.* **2010**, *105* (9), 093601.

(14) Clark, S. M.; Fu, K. M. C.; Ladd, T. D.; Yamamoto, Y. Quantum Computers Based on Electron Spins Controlled by Ultrafast Off-Resonant Single Optical Pulses. *Phys. Rev. Lett.* **2007**, *99* (4), 2−5.

(15) Grim, J. Q.; Bracker, A. S.; Zalalutdinov, M.; Carter, S. G.; Kozen, A. C.; Kim, M.; Kim, C. S.; Mlack, J. T.; Yakes, M.; Lee, B.; Gammon, D. Scalable in Operando Strain Tuning in Nanophotonic Waveguides Enabling Three-Quantum-Dot Superradiance. *Nat. Mater.* **2019**, *18* (9), 963−969.

(16) Piermarocchi, C.; Chen, P.; Sham, L. J.; Steel, D. G. Optical RKKY Interaction between Charged Semiconductor Quantum Dots. *Phys. Rev. Lett.* **2002**, *89* (16), 167402.

(17) Scheibner, M.; Ponomarev, I. V.; Stinaff, E. A.; Doty, M. F.; Bracker, A. S.; Hellberg, C. S.; Reinecke, T. L.; Gammon, D. Photoluminescence Spectroscopy of the Molecular Biexciton in

Vertically Stacked InAs-GaAs Quantum Dot Pairs. *Phys. Rev. Lett.* **2007**, *99* (19), 197402.
(18) Economou, S. E.; Reinecke, T. L. Optically Induced Spin Gates in Coupled Quantum Dots Using the Electron-Hole Exchange Interaction. *Physical Review B - Condensed Matter and Materials Physics* **2008**, *78* (11), 115306.
(19) Saikin, S. K.; Emary, C.; Steel, D. G.; Sham, L. J. Adiabatic Optical Entanglement between Electron Spins in Separate Quantum Dots. *Phys. Rev. B* **2008**, *78* (23), 235314.
(20) Trifunovic, L.; Dial, O.; Trif, M.; Wootton, J. R.; Abebe, R.; Yacoby, A.; Loss, D. Long-Distance Spin-Spin Coupling via Floating Gates. *Physical Review X* **2012**, *2* (1), 1−13.
(21) Zajac, D. M.; Sigillito, A. J.; Russ, M.; Borjans, F.; Taylor, J. M.; Burkard, G.; Petta, J. R. Resonantly Driven CNOT Gate for Electron Spins. *Science* **2018**, *359* (6374), 439−442.
(22) Mohan, A.; Gallo, P.; Felici, M.; Dwir, B.; Rudra, A.; Faist, J.; Kapon, E. Record-Low Inhomogeneous Broadening of Site-Controlled Quantum Dots for Nanophotonics. *Small* **2010**, *6* (12), 1268−1272.
(23) Holmes, M. J.; Zhu, T.; Massabuau, F. C. P.; Jarman, J.; Oliver, R. A.; Arakawa, Y. Pure Single-Photon Emission from an InGaN/GaN Quantum Dot. *APL Materials* **2021**, *9* (6), 061106.
(24) Jemsson, T.; Machhadani, H.; Karlsson, K. F.; Hsu, C.-W.; Holtz, P.-O. Linearly Polarized Single Photon Antibunching from a Site-Controlled InGaN Quantum Dot. *Appl. Phys. Lett.* **2014**, *105* (8), 081901.
(25) Cho, J.-H.; Kim, Y. M.; Lim, S.-H.; Yeo, H.-S.; Kim, S.; Gong, S.-H.; Cho, Y.-H. Strongly Coherent Single-Photon Emission from Site-Controlled InGaN Quantum Dots Embedded in GaN Nanopyramids. *ACS Photonics* **2018**, *5* (2), 439−444.
(26) Deshpande, S.; Frost, T.; Hazari, A.; Bhattacharya, P. Electrically Pumped Single-Photon Emission at Room Temperature from a Single InGaN/GaN Quantum Dot. *Appl. Phys. Lett.* **2014**, *105* (14), 141109.
(27) Deshpande, S.; Heo, J.; Das, A.; Bhattacharya, P. Electrically Driven Polarized Single-Photon Emission from an InGaN Quantum Dot in a GaN Nanowire. *Nat. Commun.* **2013**, *4* (1), 1675.
(28) Zhang, L.; Teng, C.-H.; Hill, T. A.; Lee, L.-K.; Ku, P.-C.; Deng, H. Single Photon Emission from Site-Controlled InGaN/GaN Quantum Dots. *Appl. Phys. Lett.* **2013**, *103* (19), 192114.
(29) Zhang, L.; Teng, C.; Ku, P.; Deng, H. Site-Controlled InGaN/GaN Single-Photon-Emitting Diode. *Appl. Phys. Lett.* **2016**, *108*, 153102.
(30) Teng, C.-H.; Zhang, L.; Hill, T. A.; Demory, B.; Deng, H.; Ku, P.-C. Elliptical Quantum Dots as On-Demand Single Photons Sources with Deterministic Polarization States. *Appl. Phys. Lett.* **2015**, *107* (19), 191105.
(31) Zhang, L.; Teng, C.-H.; Ku, P.-C.; Deng, H. Charge-Tunable Indium Gallium Nitride Quantum Dots. *Phys. Rev. B* **2016**, *93* (8), 085301.
(32) Chuang, S.; Chang, C. K·p Method for Strained Wurtzite Semiconductors. *Phys. Rev. B* **1996**, *54* (4), 2491.
(33) Teng, C.-H.; Zhang, L.; Deng, H.; Ku, P.-C. Mechanisms of Inhomogeneous Broadening in InGaN Dot-in-Wire Structures. *J. Appl. Phys.* **2019**, *126* (8), 083104.
(34) Borri, P.; Langbein, W.; Schneider, S.; Woggon, U.; Sellin, R.; Ouyang, D.; Bimberg, D. Ultralong Dephasing Time in InGaAs Quantum Dots. *Phys. Rev. Lett.* **2001**, *87* (15), 157401.
(35) Arita, M.; le Roux, F.; Holmes, M. J.; Kako, S.; Arakawa, Y. Ultraclean Single Photon Emission from a GaN Quantum Dot. *Nano Lett.* **2017**, *17* (5), 2902−2907.
(36) Zhang, Q.; Dang, C.; Urabe, H.; Wang, J.; Sun, S.; Nurmikko, A. Large Ordered Arrays of Single Photon Sources Based on II−VI Semiconductor Colloidal Quantum Dot. *Opt. Express* **2008**, *16* (24), 19592.
(37) Lin, X.; Dai, X.; Pu, C.; Deng, Y.; Niu, Y.; Tong, L.; Fang, W.; Jin, Y.; Peng, X. Electrically-Driven Single-Photon Sources Based on Colloidal Quantum Dots with near-Optimal Antibunching at Room Temperature. *Nat. Commun.* **2017**, *8* (1), 1132.

https://doi.org/10.1021/acsphotonics.2c00083
ACS Photonics 2022, 9, 1529−1534